Behavioral/Cognitive

Voluntary Motor Command Release Coincides with Restricted Sensorimotor Beta Rhythm Phases

Sara J Hussain,[1,2] Mary K Vollmer,[2] Iñaki Iturrate,[2,3] and Romain Quentin[2,4]

[1]Movement and Cognitive Rehabilitation Science Program, Department of Kinesiology and Health Education, University of Texas at Austin, Austin, Texas 78712, [2]Human Cortical Physiology and Neurorehabilitation Section, National Institute of Neurological Disorders and Stroke, Bethesda, Maryland 20892, [3]Amazon EU, Spain, and [4]MEL Group, EDUWELL Team, Lyon Neuroscience Research Center, Institut National de la Santé et de la Recherche Médicale U1028, Centre National de la Recherche Scientifique UMR5292, Université Claude Bernard Lyon 1, 69500 Bron, France

Sensory perception and memory are enhanced during restricted phases of ongoing brain rhythms, but whether voluntary movement is constrained by brain rhythm phase is not known. Voluntary movement requires motor commands to be released from motor cortex (M1) and transmitted to spinal motoneurons and effector muscles. Here, we tested the hypothesis that motor commands are preferentially released from M1 during circumscribed phases of ongoing sensorimotor rhythms. Healthy humans of both sexes performed a self-paced finger movement task during electroencephalography (EEG) and electromyography (EMG) recordings. We first estimated the time of motor command release preceding each finger movement by subtracting individually measured corticomuscular transmission latencies from EMG-determined movement onset times. Then, we determined the phase of ipsilateral and contralateral sensorimotor mu (8–12 Hz) and beta (13–35 Hz) rhythms during release of each motor command. We report that motor commands were most often released between 120 and 140° along the contralateral beta cycle but were released uniformly along the contralateral mu cycle. Motor commands were also released uniformly along ipsilateral mu and beta cycles. Results demonstrate that motor command release coincides with restricted phases of the contralateral sensorimotor beta rhythm, suggesting that sensorimotor beta rhythm phase may sculpt the timing of voluntary human movement.

Key words: **electroencephalography; motor; movement; oscillations; sensorimotor rhythms**

Significance Statement

Perceptual and cognitive function is optimal during specific brain rhythm phases. Although brain rhythm phase influences motor cortical neuronal activity and communication between the motor cortex and spinal cord, its role in voluntary movement is poorly understood. Here, we show that the motor commands needed to produce voluntary movements are preferentially released from the motor cortex during contralateral sensorimotor beta rhythm phases. Our findings are consistent with the notion that sensorimotor rhythm phase influences the timing of voluntary human movement.

Introduction

Voluntary movement allows us to effectively interact with our environment and is central to human behavior. Such movements are produced when the primary motor cortex (M1) issues descending motor commands that are transmitted to spinal motoneurons and connected effector muscles. However, M1 activity is rhythmic in nature, oscillating in both the mu (8–12 Hz) and beta (13–35 Hz) ranges (Pfurtscheller and Lopes da Silva, 1999; Pineda, 2005). These oscillations reflect rapidly alternating periods of excitation and inhibition (Pfurtscheller and Aranibar, 1979; Murthy and Fetz, 1992; Salmelin and Hari, 1994; Murthy and Fetz, 1996a,b; Pfurtscheller and Lopes da Silva, 1999) that correlate with local neuronal firing rates (Murthy and Fetz, 1996a; Haegens et al., 2011), population-level neuronal activity (Miller et al., 2012) and communication between M1 and spinal motoneurons (Mima and Hallett, 1999; Mitchell et al., 2007; Berger et al., 2014; Ferreri et al., 2014; Khademi et al., 2018; Zrenner et al., 2018; Bergmann et al., 2019; Hussain et al., 2019; Khademi et al., 2019; Torrecillos et al., 2020). Outside the motor system, oscillatory phase shapes sensory and cognitive function, including perception (Busch et al., 2009; Dugué et al., 2011; Hanslmayr et al., 2013; Baumgarten et al., 2015; VanRullen, 2016),

Received July 22, 2021; revised May 9, 2022; accepted May 11, 2022.

Author contributions: S.J.H., M.K.V., I.I., and R.Q. designed research; S.J.H., M.K.V., and R.Q. performed research; I.I. contributed unpublished reagents/analytic tools; S.J.H., M.K.V., I.I., and R.Q. analyzed data; S.J.H. wrote the paper.

This work was supported by the Intramural Research Program of the National Institute of Neurological Disorders and Stroke (NINDS). S.J.H. and R.Q. were supported by NINDS Intramural Competitive Fellowships. R.Q. was supported by the ATIP-AVENIR program. We thank the Human Cortical Physiology and Neurorehabilitation Section (directed by Leonardo Cohen) at NINDS for the data included in this work.

The authors declare no competing financial interests.

Correspondence should be addressed to Sara J Hussain at sara.hussain@austin.utexas.edu.

https://doi.org/10.1523/JNEUROSCI.1495-21.2022

attention (Busch and VanRullen, 2010; VanRullen, 2018) and memory (Kerrén et al., 2018; Ten Oever et al., 2020; Ter Wal et al., 2021). Yet, the relationship between sensorimotor oscillatory phase and voluntary motor behavior has remained largely unexplored.

Within M1, single-neuron spiking rates, population-level neuronal activity, and corticospinal motor output are all increased during restricted phases of sensorimotor mu and beta rhythms (Murthy and Fetz, 1996a; Haegens et al., 2011; Miller et al., 2012; Zrenner et al., 2018; Bergmann et al., 2019; Hussain et al., 2019; Wischnewski et al., 2022). Based on these findings, it has been proposed that oscillations in the membrane potential of the layer V pyramidal neurons that causally produce voluntary movement (Brecht et al., 2004) generate phase-dependent fluctuations in M1 activity and its output (Zrenner et al., 2018; Bergmann et al., 2019; Hussain et al., 2019). Because motor commands are only released from M1 when its activity reaches an excitatory threshold (Hanes and Schall, 1996; Chen et al., 1998), phase-dependent fluctuations in M1 activity may determine when along mu and beta oscillatory cycles motor commands are most likely to be released.

Here, we addressed this question using a combination of transcranial magnetic stimulation (TMS), electromyography (EMG), electroencephalography (EEG), and self-paced finger movements. We hypothesized that motor commands are preferentially released from M1 during restricted phase ranges of sensorimotor mu and beta rhythms. If true, contralateral but not ipsilateral sensorimotor rhythm phase during voluntary motor command release should be biased toward a specific phase range. Alternatively, if sensorimotor rhythm phase is unrelated to motor command release, contralateral and ipsilateral sensorimotor rhythm phase during motor command release should be uniformly distributed across all possible phases. We report that motor commands needed to produce self-paced finger movements were preferentially released from M1 during the falling phase of the contralateral beta cycle but were released uniformly along contralateral mu, ipsilateral mu, and ipsilateral beta cycles. Our results show that motor commands are most often released from M1 during restricted phases of sensorimotor β rhythms, suggesting that beta phase may sculpt the timing of voluntary human movement.

Material and Methods

Data acquisition

Subjects and experimental design. Twenty-one healthy subjects participated in this study (11 female, 10 male, age = 27.66 ± 5.01 years old [mean ± SD]). This sample size was selected as recent work has detected phase-dependent variation in corticospinal motor output with sample sizes between 12 and 23 (Zrenner et al., 2018; Bergmann et al., 2019; Hussain et al., 2019; Torrecillos et al., 2020). This study was approved by the National Institutes of Health Combined Neuroscience Section Institutional Review Board. Before participation, all subjects provided their written informed consent. This study involved a combination of single-pulse TMS, EEG, EMG, and behavioral testing.

EEG and EMG recording. Sixty-four-channel EEG signals (ground, O10; reference, AFz) and bipolar EMG signals (ground, dorsum of left wrist) were recorded using TMS-compatible amplifiers (NeurOne Tesla, Bittium) at 5 kHz (low-pass hardware filtering cutoff frequency, 1250 Hz; resolution, 0.001 μV) during single-pulse TMS delivery and during the self-paced finger movement task. EEG impedances were maintained below 10 kΩ, and EMG was recorded from the left first dorsal interosseous muscle (L FDI) using disposable adhesive electrodes arranged in a belly-tendon montage.

Single-pulse TMS delivery. The scalp hotspot for the L FDI muscle was identified over the hand representation of the right M1 as the site that elicited the largest motor-evoked potential (MEP) and a visible, focal twitch in the L FDI muscle following suprathreshold single-pulse TMS. Resting motor threshold (RMT) was determined using an automatic threshold-tracking algorithm (Adaptive PEST Procedure, MTAT 2.0, https://www.clinicalresearcher.org/software.htm). Then, 50 single TMS pulses were delivered to the L FDI hotspot at 120% RMT (interpulse interval, 6 s with 0.9 s jitter). The MEP latency was defined as the amount of time needed for action potentials produced by TMS to travel from the stimulated M1 to the L FDI muscle (see below, EMG processing). All TMS procedures were performed using a figure-of-eight coil held at ~45° relative to the midsagittal line (MagStim Rapid^2, biphasic pulse shape). RMT was 61.62 ± 12.27% (mean ± SD) of maximum stimulator output.

Self-paced finger movement task. Subjects performed a self-paced voluntary finger movement task during which they viewed a series of unique pictures on a computer screen (Places Scene Recognition Database; Zhou et al., 2018; Fig. 1*a*). A self-paced movement task rather than an externally paced (e.g., visually cued) reaction time task was used because sensory perception of a stimulus varies with oscillatory phase (Busch et al., 2009; Hanslmayr et al., 2013; Baumgarten et al., 2015; VanRullen, 2016). Using a self-paced movement task therefore eliminates the possibility that any phase-dependent motor command release observed in the current study could be confounded by phase-dependent variation in sensory perception of the stimulus.

During the self-paced finger movement task, subjects were instructed to view each picture for as long as they desired and then use their left index finger to press a button on a standard keyboard (left CTRL button) when they wished to view the next picture in the series. Between pictures, a fixation cross was presented (intertrial interval, 1.5 s with 0.2 s jitter). The task was designed to ensure that subjects produced a self-paced, discrete finger movement when they desired. During the task, the left arm was supported on a pillow to ensure full muscle relaxation and prevent extraneous movement. The finger movement task was divided into six blocks of 100 unique pictures. Subjects were given a short break after three blocks. To ensure that subjects were not merely reacting as fast as possible to the presentation of each picture and that movements were truly self-paced, trials with reaction times faster than 400 ms were excluded from further analysis (see below, Experimental design and statistical analysis).

Data analysis

EMG processing. EMG signals were processed using FieldTrip software (Oostenveld et al., 2011) combined with custom-written scripts (MATLAB, MathWorks). EMG signals were used to (1) measure MEP latencies obtained using single-pulse TMS and (2) determine movement onset during the finger movement task.

To measure MEP latencies, data were divided into segments (−0.25 to +0.100 s relative to TMS pulse), demeaned, and linearly detrended. For each subject, MEP signals were averaged over trials to generate a mean MEP signal. The inflection point between poststimulus baseline EMG activity and the beginning

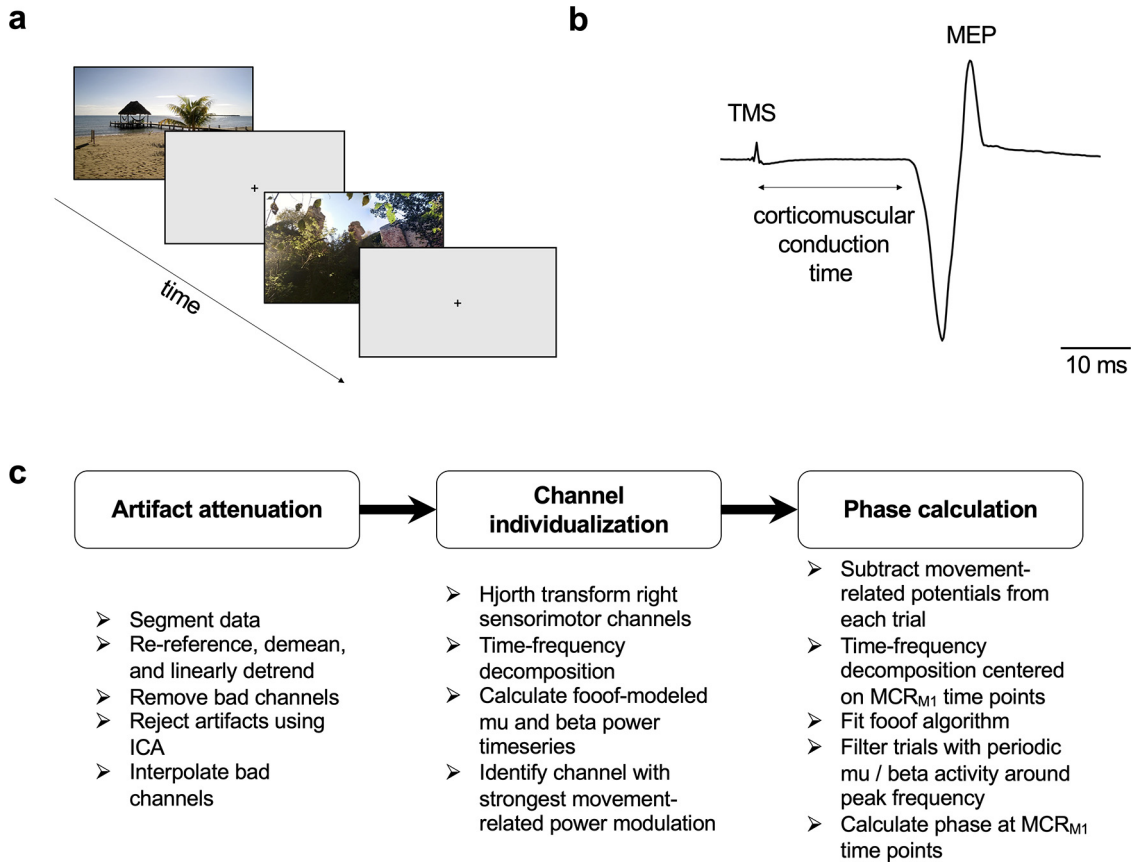

Figure 1. Experimental design and EEG analysis approach. ***a***, Subjects viewed a series of pictures on a computer screen while they performed a self-paced finger movement task. Subjects were instructed to press a button using their left index finger when they wished to move to the next picture. EMG and EEG signals were recorded during the task. ***b***, Before task performance, single-pulse TMS was used to determine each subject's corticomuscular conduction time by measuring the L FDI MEP onset latency. Corticomuscular conduction times were used to identify the time of motor command release from M1 preceding each finger movement. ***c***, Flowchart depicting EEG processing steps.

of the mean MEP waveform was visually identified as the MEP latency (Fig. 1*b*). For two subjects in whom MEP latencies could not be reliably identified, MEP latencies were set equal to the mean latency obtained in all other subjects. At the group level, MEP latencies were 23.49 ± 1.73 ms (mean ± SD; range, 20.4–26.8, Table 1).

To measure movement onset, EMG data were divided into 2.4 s segments (± 1.2 s relative to the button press during the task) demeaned, and linearly detrended. A notch filter (zero-phase shift Butterworth filter; order 4, stop band 58–60 Hz) was applied to remove line noise, followed by a high-pass filter (zero-phase shift Butterworth filter; order 6, cutoff frequency 20 Hz, De Luca et al., 2010). Voluntary EMG activity onset for each button press was visually identified using a combination of frequency- and time-domain EMG analysis. EMG signals were spectrally decomposed over time (multitaper method using Hanning tapers, 20–500 Hz, time window 0.100 s, 0.2 ms resolution). To identify voluntary EMG onsets preceding each button press, trimmed EMG time-frequency representations (−1.2 s to 0 s, where 0 s reflects the button press) were plotted alongside time series EMG but not EEG signals. The experimenter identifying EMG onsets (M.K.V.) was thus blinded to EEG activity during EMG onset identification and did not analyze EEG signals. EMG onsets were detected by first localizing the general latency at which the time-frequency representation of each movement showed increased EMG power across multiple frequencies. Then, the experimenter examined the corresponding general latency of the time series EMG signal to detect the exact time point at which the signal visually deviated from background noise (Figs. 2*c–f*, 3*c–f*; note that some temporal smearing of EMG power occurs because of the 100 ms window used during time-frequency decomposition of EMG signals). During EMG onset detection, we noted that L FDI muscle activity did not return to quiet baseline after many movements, precluding reliable EMG onset detection of the following movement. These trials were excluded from further analysis (see below, Experimental design and statistical analysis).

EEG processing. EEG signals were processed with FieldTrip (Oostenveld et al., 2011) and custom-written MATLAB scripts (MathWorks). Signals recorded during the finger movement task were divided into 2.4 s segments (± 1.2 s relative to the button press). Segmented data were rereferenced to the average reference, demeaned, and linearly detrended. Channels with impedances >10 kΩ were removed, and independent components analysis (ICA) was used to attenuate EEG artifacts. ICA was applied using the infomax algorithm (Bell and Sejnowski, 1995) in all subjects except four in whom this approach did not converge. In these four, the FastICA algorithm was used instead (Hyvarinen, 1999). After ICA, components with scalp topographies reflecting EEG artifacts (i.e., eye movements, eyeblinks, electrode noise, etc.) were rejected, and all remaining components were back projected into EEG sensor space (on average, 5.33 ± 0.61 [mean ± SD] components were rejected per subject).

After ICA, channels previously removed because of high impedances were interpolated using spherical splines, and a

Table 1. Individual MEP latencies, center frequencies, and fooof model fits

		Individual frequencies (Hz)				Fooof fits (r^2)			
		Contralateral		Ipsilateral		Contralateral		Ipsilateral	
Subject	MEP latency (ms)	Mu	Beta	Mu	Beta	Mu	Beta	Mu	Beta
1	25.0	10.64 (1.18)	20.16 (4.41)	10.92 (1.15)	22.54 (4.84)	0.86 (0.13)	0.74 (0.19)	0.79 (0.15)	0.77 (0.19)
2	22.8	10.35 (1.10)	20.61 (4.58)	11.13 (1.23)	21.40 (4.21)	0.83 (0.10)	0.79 (0.18)	0.81 (0.20)	0.83 (0.10)
3	22.2	10.87 (1.32)	20.62 (5.64)	10.85 (1.13)	21.58 (5.58)	0.79 (0.15)	0.79 (0.17)	0.83 (0.15)	0.84 (0.16)
4	22.0	10.93 (1.06)	20.68 (5.80)	11.10 (1.13)	22.45 (5.76)	0.90 (0.11)	0.82 (0.17)	0.85 (0.10)	0.77 (0.20)
5	—	10.94 (1.04)	22.35 (5.43)	11.43 (1.05)	22.59 (4.71)	0.87 (0.11)	0.87 (0.14)	0.92 (0.09)	0.90 (0.11)
6	26.2	10.61 (1.11)	22.31 (5.93)	10.94 (1.10)	22.38 (5.18)	0.81 (0.13)	0.79 (0.18)	0.82 (0.11)	0.83 (0.17)
7	23.8	—	—	—	—	—	—	—	—
8	22.6	11.67 (0.78)	21.09 (5.04)	—	—	0.85 (0.10)	0.80 (0.14)	—	—
9	20.4	—	—	11.29 (1.24)	21.45 (5.57)	—	—	0.80 (0.15)	0.76 (0.17)
10	26.8	10.55 (0.89)	23.40 (6.50)	10.12 (0.78)	24.46 (5.97)	0.86 (0.12)	0.83 (0.14)	0.87 (0.15)	0.78 (0.17)
11	—	11.67 (1.12)	—	11.81 (1.14)	22.20 (5.78)	0.88 (0.12)	—	0.89 (0.12)	0.89 (0.08)
12	23.4	11.10 (1.08)	21.44 (5.69)	11.30 (1.23)	21.16 (5.05)	0.79 (0.15)	0.78 (0.17)	0.82 (0.14)	0.77 (0.16)
13	23.2	11.27 (0.86)	25.15 (4.90)	11.04 (0.94)	22.52 (5.67)	0.86 (0.13)	0.85 (0.16)	0.83 (0.11)	0.81 (0.19)
14	22.4	11.21 (1.07)	20.72 (4.20)	11.07 (0.87)	20.99 (3.65)	0.89 (0.12)	0.88 (0.12)	0.93 (0.10)	0.89 (0.09)
15	23.4	10.69 (1.26)	19.85 (5.31)	11.33 (0.96)	20.07 (5.11)	0.86 (0.12)	0.75 (0.17)	0.86 (0.11)	0.77 (0.14)
16	24.6	10.75 (1.04)	21.91 (5.64)	11.01 (1.18)	21.96 (6.51)	0.83 (0.12)	0.80 (0.17)	0.82 (0.16)	0.73 (0.24)
17	21.6	10.62 (1.04)	23.89 (5.43)	10.41 (0.76)	24.32 (5.51)	0.88 (0.12)	0.84 (0.16)	0.85 (0.11)	0.86 (0.13)
18	26.2	10.41 (1.32)	22.25 (5.06)	10.79 (0.95)	21.58 (5.64)	0.80 (0.17)	0.81 (0.16)	0.88 (0.09)	0.87 (0.10)
19	25.0	11.37 (1.24)	21.60 (6.58)	11.84 (1.00)	20.08 (6.58)	0.82 (0.18)	0.87 (0.11)	0.86 (0.12)	0.88 (0.12)
20	22.8	—	20.26 (4.23)	—	23.10 (5.79)	—	0.82 (0.16)	—	0.83 (0.13)
21	22.0	—	—	11.02 (1.22)	23.88 (6.34)	—	—	0.84 (0.13)	0.85 (0.13)
Mean	23.49	10.92	21.66	11.08	22.20	0.85	0.81	0.85	0.82
SD	1.73	0.41	1.44	0.42	1.26	0.03	0.04	0.04	0.05

For MEP latencies, dashes depict subjects for whom latencies could not be reliably identified. For all other columns, dashes depict subjects with fewer than 10 trials per hemisphere and frequency.

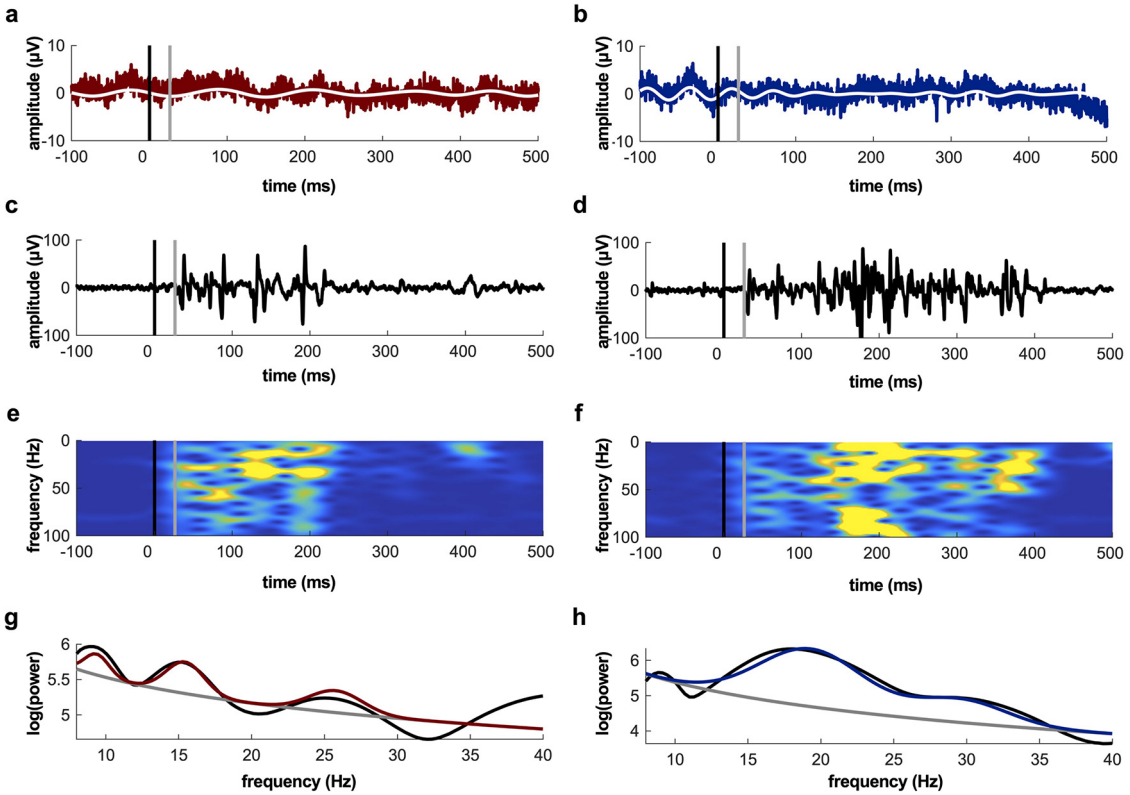

Figure 2. EMG and contralateral EEG data during individual finger movements recorded from a representative subject. ***a***, ***b***, Raw (colored) and bandpass-filtered (white) contralateral EEG data during individual finger movements. ***c***, ***d***, Time-domain representation of L FDI EMG data during individual finger movements. ***e***, ***f***, Time-frequency representation of L FDI EMG data during individual finger movements. Cooler and warmer colors indicate smaller and larger values, respectively. Note that color scaling was chosen to emphasize the onset of EMG activity. ***g***, ***h***, Raw power spectra (black), aperiodic fit of raw power spectra (gray), and fooof-modeled power spectra (colored). Black lines indicate MCR_{M1} time points, and gray lines indicate EMG onset time points (***a–f***). Left, contralateral mu; right, contralateral beta. Note the oscillatory activity present in all raw EEG traces (***a***, ***b***) and power spectra (***g***, ***h***) for mu and beta, respectively.

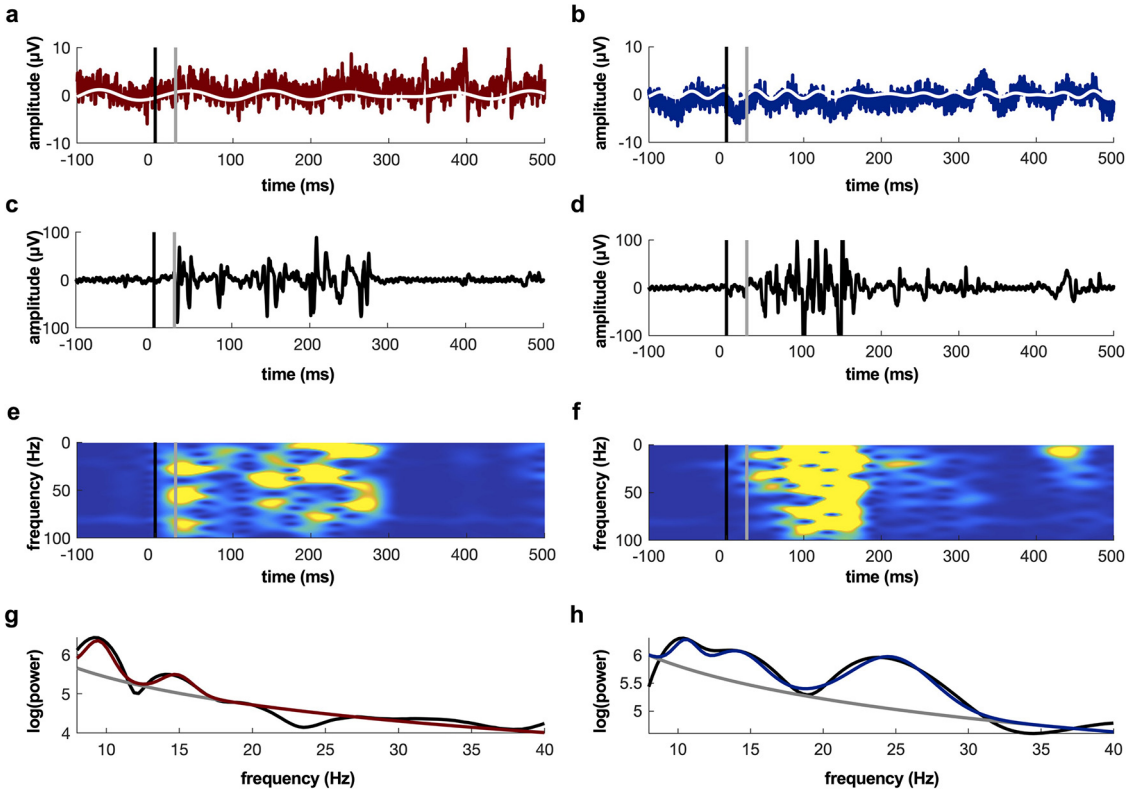

Figure 3. EMG and ipsilateral EEG data during individual finger movements recorded from a representative subject. ***a***, ***b***, Raw (colored) and bandpass-filtered (white) ipsilateral EEG data during individual finger movements. ***c***, ***d***, Time domain L FDI EMG data during individual finger movements. ***e***, ***f***, Time-frequency representation of L FDI EMG data during individual finger movements. Cooler and warmer colors indicate smaller and larger values, respectively. Note that color scaling was chosen to emphasize the onset of EMG activity. ***g***, ***h***, Raw power spectra (black), aperiodic fit of raw power spectra (gray), and fooof-modeled power spectra (colored). Black lines indicate MCR_{M1} time points and gray lines indicate EMG onset time points (***a–f***), Left, ipsilateral mu; right, ipsilateral beta. Note the oscillatory activity present in all raw EEG traces (***a***, ***b***) and power spectra (***g***, ***h***) for mu and beta, respectively.

subset of channels overlying the right sensorimotor cortex (contralateral to the L FDI; FC2, FC4, FC6, Cz, C2, C4, C6, T8, CP2, CP4, CP6) and the left sensorimotor cortex (ipsilateral to the L FDI; FC1, FC3, FC5, Cz, C1, C3, C5, T7, CP1, CP3, CP5) were selected for further analysis. Each selected channel and its four neighbors were then used to obtain Hjorth-transformed EEG signals (Hjorth, 1975) by subtracting the average of the four neighboring surround channels from the central channel at each time point (Zrenner et al., 2018; Hussain et al., 2019). This approach attenuates the effects of volume conduction and enhances the signal-to-noise ratio of local EEG features (Hjorth, 1975).

We individualized the Hjorth-transformed scalp channels used for mu and beta analysis by identifying those that best captured movement-related mu and beta reactivity (Torrecillos et al., 2020) over the contralateral hemisphere. To achieve this, we first performed time-frequency analysis (wavelet method using Hanning tapers, width 7, 8–40 Hz with 0.25 Hz resolution, 1 Hz smoothing, 0.2 ms resolution [5 kHz]) on EEG data from channels overlying the right sensorimotor cortex. Afterward, we parameterized the power spectrum of each time point per channel into periodic and aperiodic components using the fooof algorithm (Donoghue et al., 2020). Briefly, this algorithm decomposes power spectra into their aperiodic components (reflected as the general 1/f trend of the spectrum) and periodic components (reflected as peaks that exceed the 1/f trend). The rationale for this decomposition is that these different components are related to distinct neural processes, with periodic components reflecting rhythmic oscillatory activity (Donoghue et al., 2020) and the aperiodic component estimating population-level neuronal spiking (Manning et al., 2009) and synaptic excitation-inhibition balance (Gao et al., 2017). The fooof algorithm fits power spectra using an aperiodic component combined with multiple gaussians (Donoghue et al., 2020, their Fig. 2) and allows the user to set its parameters, including the maximum number of peaks and the minimum peak height. The maximum number of peaks was set to 4 to account for up to four possible spectral peaks between 8 and 40 Hz. To avoid misidentifying noisy EEG epochs as periodic oscillatory activity, the minimum peak height was set to 0.1. Peak width limits were set to 0.5–12 Hz, and the peak threshold was set to 2.0 (Donoghue et al., 2020, refer to their Supplementary Table 2 for default fooof algorithm parameter values). Center frequencies and the number of detected spectral peaks tended to be more consistent across different time points of the same trial than across different trials (Table 2).

To characterize the role of rhythmic oscillatory phase in human motor command release, all subsequent spectral analyses were performed using the fooof algorithm (Donoghue et al., 2020). At each time point, fooof-modeled power values were averaged in the mu (8–12 Hz) and beta (13–35 Hz) ranges, generating fooof-modeled mu and beta power time series signals. These signals were subsequently smoothed (moving average, time window = 50 ms), and the channel showing the strongest movement-related power modulation within ± 750 ms of the button press was identified separately for mu and beta. Time series signals were also visually inspected to ensure appropriate channel selection. One channel was selected per subject and frequency. This channel was used for analysis of oscillatory phase within the contralateral hemisphere. For mu, Cz, C2, C6, T8, and

Table 2. Group-level coefficients of variation for center frequencies and the number of spectral peaks detected by the fooof algorithm

	Coefficient of variation of center frequencies				Coefficient of variation of number of detected peaks			
	Contralateral		Ipsilateral		Contralateral		Ipsilateral	
Calculation method	Mu	Beta	Mu	Beta	Mu	Beta	Mu	Beta
Across time points within the same trial	0.01 (0.004)	0.03 (0.01)	0.01 (0.004)	0.03 (0.02)	0.17 (0.06)	0.16 (0.04)	0.14 (0.04)	0.15 (0.03)
Across trials at MCR_{M1} time points	0.10 (0.02)	0.25 (0.03)	0.10 (0.01)	0.25 (0.06)	0.37 (0.05)	0.41 (0.04)	0.34 (0.09)	0.42 (0.09)

Coefficients of variation were calculated per trial at each time point within ± 5 ms of MCR_{M1} (top row) and across trials at MCR_{M1} (bottom row).

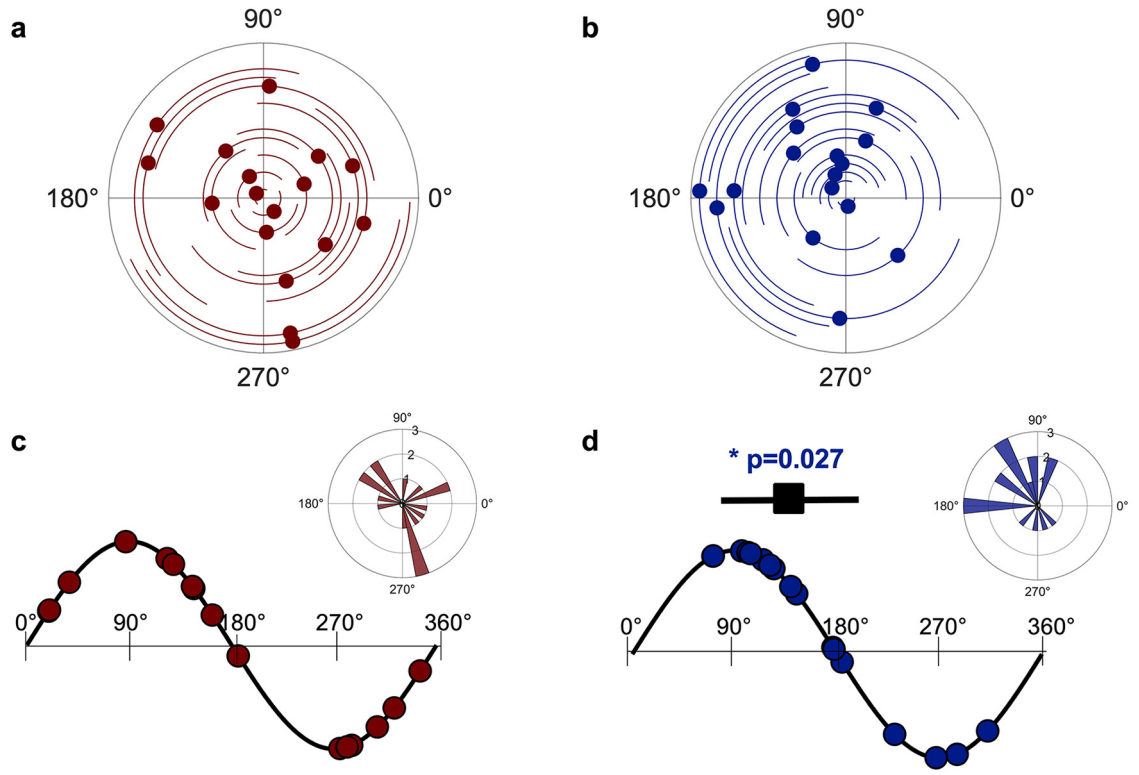

Figure 4. Contralateral mu and beta phase angles during MCR_{M1}. ***a***, ***b***, Variation in phase angles during MCR_{M1} at the individual subject level for contralateral mu (***a***) and beta (***b***) rhythms. Each dot reflects an individual subject's mean phase angle during MCR_{M1}. Each circular line reflects an individual subject's phase angle SD during MCR_{M1}. ***c***, ***d***, Mu (***c***) and beta (***d***) phase angles during MCR_{M1} along the oscillatory cycle and in phase space. Each dot indicates a single subject's mean phase angle during MCR_{M1}. Phase angle histograms represent group-level distributions of mean phase angles during MCR_{M1}. Radii values indicate the number of subjects showing mean phase angles within a given phase bin. The black square and horizontal line in ***d*** reflect the mean beta phase angle and the group-level SD. For ***c***, the group mean and SD is not shown because of lack of significant deviations from uniformity. The asterisk reflects significance at $p < 0.05$.

CP2 were selected in one subject each, FC2 was selected in two subjects, CP4 was selected in three subjects, CP6 was selected in 5 subjects, and C4 was selected in six subjects. For beta, C4, C6, and T8 were each selected in one subject each, Cz and FC2 were selected in two subjects each, CP2 and CP4 were each selected in three subjects each, and CP6 was selected in eight subjects. For analysis of oscillatory phase within the ipsilateral hemisphere, the mirror-symmetric channel was used for each subject. For the subject in whom Cz was used for contralateral hemisphere analysis, C1 was used for ipsilateral analysis. Based on our main results (see below, Results; see Fig. 4), the same analysis described below (see Estimating time of motor command release from M1 [MCR_{M1}] and Phase angle calculation) was performed using the C4 channel in all participants (i.e., without individualizing channel selection) for contralateral beta. C4 phase angles did not show any deviation from uniformity at MCR_{M1} ($p = 0.27$, $z = 1.30$ for group-level mean phase angles; $p = 0.55$ and $z = 0.58$ for group-level pooled phase angles; see below, Experimental design and statistical analysis), indicating the importance of individualizing channels before analysis (Torrecillos et al., 2020; Ibáñez et al., 2021). After selecting subject-specific channels, movement-related potentials time locked to each button press were calculated for each subject. To control for the possibility that any observed phase-dependent motor command release is related to movement-related potentials, these potentials were subtracted from each EEG trial (Klimesch et al., 1998; Pellicciari et al., 2017; Premoli et al., 2017).

Estimating time of motor command release from M1 (MCR_{M1}). The time of MCR_{M1} was estimated for each finger movement by subtracting the individual MEP latency from the EMG-defined onset time of each movement (see above, EMG processing; Figs. 2, 3). Because the MEP latency reflects the amount of time needed for an action potential to travel from the stimulated M1 to the L FDI muscle involved in the self-paced movement task (i.e., corticomuscular conduction time; see above, Single-pulse TMS delivery; Fig. 1*b*), this approach provided an individualized and physiologically informed estimate of MCR_{M1} preceding each finger movement.

Phase angle calculation. If sensorimotor rhythm phase shapes voluntary motor command release, phase-dependent motor command release should only be detectable in the hemisphere contralateral to the moving finger. We therefore examined the mu and beta phase during motor command release for each hemisphere, focusing only on those finger movements in which (1) EMG onsets could be reliably detected (see above, EMG processing) and (2) periodic activity was detected within mu and beta frequencies, indicating the presence of a sustained oscillation in the target frequency. Preprocessed EEG data recorded during individual finger movements were used to identify those movements during which contralateral and ipsilateral periodic mu and beta oscillatory activity was present. Time-frequency representations were computed using the same approach described for each finger movement (see above, EEG processing). Then, the fooof-modeled power spectrum centered on the MCR_{M1} time point (see above, Estimating time of motor command release from M1 [MCR_{M1}]) was used to determine the dominant mu and beta center frequency of each finger movement in each hemisphere.

All movements containing detectable periodic components at MCR_{M1} were bandpass filtered into individually defined, movement-specific frequency ranges (one-pass finite impulse response filter with phase delay correction, window length 500 ms, order 2500, passband ± 2 Hz relative to the periodic component center frequency of each movement, rounded to the nearest integer). Movements with EEG activity containing visible artifacts not attenuated by previous ICA were excluded from further analysis. The ipsilateral and contralateral mu and beta phase angles during each MCR_{M1} time point was calculated for each movement using the Hilbert transform. Phase angles for each hemisphere and frequency were combined across all analyzed movements, and each subject's mean phase angle was computed for each frequency and hemisphere. Of note, phase angles as calculated here are in principle generated by a mixture of periodic and aperiodic activity. However, by analyzing only those finger movements with detectable periodic activity, these angles reflect the phase of a neural signal containing sensorimotor mu and/or beta rhythms. Figures 2 and 3 contain EEG and EMG data obtained from a representative subject during self-paced finger movements.

Experimental design and statistical analysis

After removing trials in which subjects reacted to picture presentation too quickly (see above, Self-paced finger movement task), on average 587.57 ± 40.19 (mean ± SD) trials (range, 417–600) were available for analysis per subject. After removing trials in which reliable EMG onsets could not be detected because of inadequate L FDI relaxation between trials (see above, EMG processing), 139.29 ± 88.39 trials (range, 29–335) were available for analysis. Finally, 34.90 ± 25.00 of these trials (range, 0–80) contained contralateral mu periodic activity, 78.48 ± 75.47 contained contralateral beta periodic activity (range, 0–294), 34.33 ± 22.82 contained ipsilateral mu periodic activity (range, 1–84), and 82.10 ± 73.85 contained ipsilateral beta activity (range, 17–306; see above, EEG processing and Phase angle calculation). These trials were used for final statistical analysis. Further, some subjects had fewer than 10 trials available for a given hemisphere and frequency band; these subjects were excluded from statistical analyses for that hemisphere and frequency (contralateral mu, four subjects excluded; contralateral beta, four subjects excluded; ipsilateral mu, three subjects excluded; ipsilateral beta, two subjects excluded).

We tested whether phase angles during MCR_{M1} immediately preceding self-paced finger movements preferentially clustered within restricted phase ranges of the mu and beta rhythms using circular statistics. At the individual level, phase angles during MCR_{M1} were tested for unimodal deviations from uniformity using the Rayleigh test for each frequency and hemisphere. At the group level, we concatenated the mean phase angles obtained for each subject during MCR_{M1} across all subjects for each frequency and hemisphere. As a secondary group-level analysis, we also pooled phase angles during MCR_{M1} across all subjects within the mu and beta ranges by concatenating them to create a group-level pooled phase angle distribution for each hemisphere. This was done to control for the possibility that our subject-specific phase angle averaging procedure may have biased our results. All group-level frequency- and hemisphere-specific phase distributions were tested for unimodal deviations from uniformity using the Rayleigh test. Statistical analyses were performed in MATLAB using custom-written scripts combined with the CircStat Toolbox (Berens, 2009). Alpha was equal to 0.05 for all statistical tests. All reported summary statistics are mean ± SD.

Data availability

Data and code used in this study are available from the corresponding author on reasonable request.

Results

We first determined whether MCR_{M1} required to produce self-paced voluntary finger movements preferentially occurred during restricted phase ranges of contralateral, right hemisphere sensorimotor rhythms. Contralateral mu and beta activity during self-paced finger movements oscillated at 10.91 ± 0.41 Hz and 21.72 ± 1.43 Hz, respectively. At the individual subject level, contralateral phase angles at MCR_{M1} time points deviated from uniformity in one subject for mu ($z = 3.86$, $p = 0.02$) and one subject for beta ($z = 6.99$, $p = 0.001$; all others $z < 2.97$, $p > 0.05$), likely because of low statistical power. At the group level, mean beta phase angles during MCR_{M1} exhibited a significant, unimodal deviation from uniformity at 137.58 ± 59.80° ($z = 3.52$, $p = 0.027$; Fig. 4*b*,*d*), which coincides with the falling phase of the beta cycle. Consistent with this, the pooled group-level distribution of contralateral beta phase angles during MCR_{M1} also deviated from uniformity within the falling phase (124.95 ± 79.22°, $z = 3.19$, $p = 0.041$). In contrast, neither mean contralateral mu phase angles or the pooled group-level distribution of contralateral mu phase angles during MCR_{M1} significantly differed from uniformity (Fig. 4*a*,*c*; $z < 1.30$, $p > 0.27$ for both). Thus, contralateral phase angles during motor command release were biased between 120 and 140° (i.e., the falling phase) of the beta but not the mu oscillatory cycle.

If sensorimotor rhythm phase influences voluntary motor command release, a relationship between sensorimotor rhythm phase and MCR_{M1} time points should only be present for the contralateral right hemisphere. We therefore also tested whether MCR_{M1} time points clustered near any specific oscillatory phase recorded from the ipsilateral left hemisphere. During self-paced finger movements, ipsilateral mu and beta rhythms oscillated at 11.09 ± 0.39 Hz and 22.19 ± 1.21 Hz, respectively. At the individual subject level, ipsilateral mu and beta phase angles at MCR_{M1} time points deviated from uniformity in one subject each (mu, $z = 4.94$, $p = 0.006$; beta, $z = 3.26$, $p = 0.037$; all others $z <$

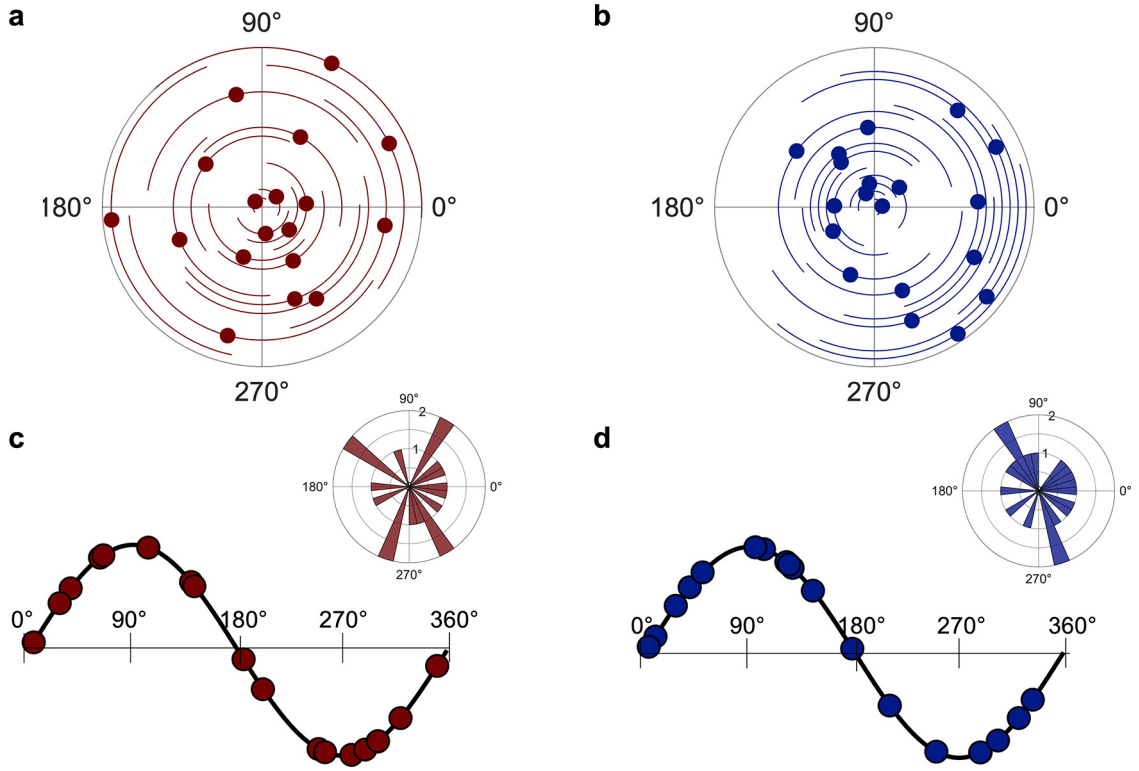

Figure 5. Ipsilateral mu and beta phase angles during MCR_{M1}. Variation in phase angles during MCR_{M1} at the individual subject level for ipsilateral mu (***a***) and beta (***b***). Each dot reflects an individual subject's mean phase angle during MCR_{M1}. Each circular line reflects an individual subject's phase angle SD during MCR_{M1}. ***c***, ***d***, Mu (***c***) and beta (***d***) phase angles during MCR_{M1} along the oscillatory cycle and in phase space. Each dot indicates a single subject's mean phase angle during MCR_{M1}. Phase angle histograms represent group-level distributions of mean phase angles during MCR_{M1}. Radii values indicate the number of subjects showing mean phase angles within a given phase bin. For ***c*** and ***d***, group means and SDs are not shown because of lack of significant deviations from uniformity.

2.46, $p > 0.08$). At the group level, neither the mean nor pooled group-level distribution of ipsilateral phase angles during MCR_{M1} deviated significantly from uniformity for either frequency (Fig. 5; $z < 1.09$, $p > 0.33$ for all). Thus, phase angles during motor command release were not biased toward any specific phase range of either the ipsilateral mu or beta cycle.

We also performed all group-level analyses on EEG data from which movement-related potentials were not subtracted. In the contralateral hemisphere, mu and beta rhythms oscillated at 10.98 ± 0.39 Hz and 21.87 ± 1.27 Hz, respectively. Group-level mean beta phase angles at MCR_{M1} time points deviated significantly from uniformity at 115.67 ± 62.31° ($z = 3.00$, $p = 0.047$), whereas this was not the case for group-level mean mu phase angles ($z = 1.67$, $p = 0.19$). Group-level pooled phase angles did not deviate from uniformity for either mu or beta ($z < 2.46$, $p < 0.11$). In the ipsilateral hemisphere, mu and beta rhythms oscillated at 11.05 ± 0.38 Hz and 21.92 ± 1.87 Hz, respectively. Group-level mean and pooled phase angles at MCR_{M1} time points did not deviate from uniformity for either mu or beta ($z < 0.63$, $p > 0.52$).

Discussion

We tested the hypothesis that motor commands required to produce self-paced finger movements are preferentially released from M1 during restricted phase ranges of ongoing sensorimotor rhythms. If so, contralateral but not ipsilateral phase angles during motor command release should be biased toward a specific oscillatory phase. To evaluate this hypothesis, we first estimated the time at which motor commands needed to produce self-paced finger movements were released from M1 using a combination of TMS, EEG, EMG, and behavioral testing. Then, we calculated the contralateral and ipsilateral mu and beta oscillatory phase angles at the identified time of motor command release. Consistent with our hypothesis, phase angles during MCR_{M1} were nonuniformly distributed across all phase angles for the contralateral beta cycle but uniformly distributed for the contralateral mu cycle. Moreover, phase angles during MCR_{M1} were evenly distributed across ipsilateral mu and beta cycles. These results were largely consistent regardless of whether movement-related potentials were subtracted from EEG signals before analysis. Our results thus show that the release of motor commands from M1, a requirement for voluntary movement, is beta phase-dependent.

Sensorimotor beta oscillatory activity covaries with M1 single-neuron spiking rates (Murthy and Fetz, 1996a; Zanos et al., 2018), M1 population-level neuronal activity (Miller et al., 2012), and corticospinal output (Mitchell et al., 2007; Berger et al., 2014; Ferreri et al., 2014; Khademi et al., 2018; Torrecillos et al., 2020), all of which are necessary for voluntary movement. In addition, corticospinal communication during voluntary movement occurs through phase synchronization of cortical and spinal rhythms (i.e., corticomuscular coherence; Farmer et al., 1993; Conway et al., 1995; Mima and Hallett, 1999; Womelsdorf et al., 2007). Outside the motor domain, perceptual function is enhanced at specific phases of oscillatory activity recorded from task-relevant brain regions (Busch et al., 2009; Dugué et al., 2011; Hanslmayr et al., 2013; Busch and VanRullen, 2010; Baumgarten et al., 2015; VanRullen, 2016; but see Ruzzoli et al., 2019), suggesting that human perception occurs through rhythmic, phase-

dependent sampling of the environment (VanRullen, 2016). Our results demonstrate that voluntary human motor output exhibits similar rhythmicity.

Motor commands were most often released from M1 during the falling phase of the ongoing beta cycle but were released uniformly across the mu cycle. Why might motor command release be coupled to the beta but not mu rhythm, and why to the falling phase? Mu and beta rhythms are generated by distinct neural mechanisms (Stolk et al., 2019). Mu rhythms localize to the primary somatosensory cortex (Salmelin and Hari, 1994), exhibit little if any somatotopy (Salmelin et al., 1995) and travel caudorostrally across the cortex (Stolk et al., 2019). In contrast, beta rhythms localize to the primary motor cortex (Salmelin and Hari, 1994), exhibit more precise somatotopic organization (Salmelin and Hari, 1994; Salmelin et al., 1995), and travel rostrocaudally across the cortex (Stolk et al., 2019). Further, beta activity is closely tied to movement initiation, as entraining beta oscillations slows movement (Pogosyan et al., 2009), and patients with Parkinson's disease often exhibit exaggerated beta activity that correlates with bradykinesia and movement initiation deficits (Little and Brown, 2014; Martin et al., 2018). Corticomuscular coherence is also strongest in the beta range (Conway et al., 1995; Baker et al., 1997; Mima and Hallett, 1999), indicating the presence of a beta-specific communication channel between M1 and spinal motoneurons during voluntary motor output (van Elswijk et al., 2010; Romei et al., 2016; Khademi et al., 2018). Further, movement-related hand muscle EMG bursts have been reported to occur during sensorimotor beta trough phases (Baker et al., 1997). To observe this pattern of phase-dependent EMG activity, the motor command initiating this EMG activity would need to be released ~20–25 ms (i.e., equal to the corticomuscular conduction delay) before the sensorimotor beta trough phase. Given that beta typically oscillates near 20 Hz (see above, Results), such motor command release would likely occur between 90 and 126° of the beta cycle, which is grossly consistent with the falling beta phase identified here (Fig. 4*d*). Along these lines, recent work also showed that corticospinal excitability oscillates synchronously with the beta cycle and is maximal during falling beta phases (Wischnewski et al., 2022).

What might be the advantage of the phase-dependent motor command release observed here? Previous invasive recording studies have shown that resting population-level neuronal activity in M1 transitions from low to high activity states during beta falling phases (Miller et al., 2012) and that such background-level spiking is present during movement itself (Murthy and Fetz, 1996a). Given that motor commands are released when M1 activity reaches an excitatory threshold (Hanes and Schall, 1996), the transition from low to high background activity may bring M1 activity to this threshold, thus triggering motor command release. This may occur through beta phase-dependent activation of M1 neurons by thalamocortical projections that cause movement initiation (Takahashi et al., 2021) so that these projections only adequately excite M1 neurons when their firing coincides with beta falling phases. This possibility mirrors phase coding mechanisms discovered outside the motor domain, where the oscillatory phase at which a neuron spikes encodes behaviorally relevant information that is not reflected by spiking rate alone (Montemurro et al., 2008; Siegel et al., 2009). Our results therefore suggest that phase coding also contributes to voluntary human movement generation.

Several classic studies have demonstrated that sensorimotor rhythms weaken (i.e., desynchronize) during motor imagery, movement preparation, and movement itself (Pfurtscheller and Aranibar, 1979; Pfurtscheller and Lopes da Silva, 1999; Pfurtscheller et al., 2006). Although we identified contralateral and ipsilateral periodic mu and beta rhythms during a substantial number of self-paced finger movements, periodic mu and beta rhythms were not detected during all finger movements. When considered alongside our findings, this suggests that either (1) motor command release is only biased toward restricted contralateral beta phases during movements with detectable contralateral beta periodic activity, or (2) contralateral beta periodic activity (and thus contralateral beta phase-dependent motor command release) is present but not detectable at the scalp level during a large portion of movements. Although our data cannot definitively distinguish between these two possibilities, the most parsimonious conclusion is that the low signal-to-noise ratio of scalp EEG signals limits detection of contralateral beta periodic activity at the single trial level (Kosciessa et al., 2020).

Some limitations to the current work exist. First, we estimated the time of motor command release from M1 by quantifying each subject's corticomuscular conduction delay using TMS-evoked MEPs, which are generated by artificially evoked descending volleys (Di Lazzaro and Ziemann, 2013) after very brief M1 activation (here, 400 μs). In contrast, voluntary M1 activation is more temporally dispersed (i.e., 100–200 ms for discrete movements, Hanes and Schall, 1996). As a result, our findings only reflect beta phase-dependency of an initial voluntary descending volley, with all later volleys spread throughout subsequent beta phases. Second, our results do not imply that motor commands are only released during certain phase ranges but rather indicate that motor commands are disproportionately released during beta falling phases. Patients with bradykinesia may for example experience exaggerated phase-dependent motor command release that pathologically delays movement. Examining the relationship between phase-dependent motor command release and movement initiation deficits in patients with Parkinson's disease may shed light on this possibility. Finally, it is also possible that movement-related cortical activity alters non-phase-locked contralateral beta oscillations in a way that aligns motor command release to the falling contralateral beta phase identified here. Interventional studies that evaluate phase-dependent motor command release while also entraining the contralateral beta rhythm could address this possibility.

In sum, we report that motor commands preceding self-paced finger movements were preferentially released from M1 during the falling phase of the contralateral beta cycle between 120 and 140° but were released uniformly across the contralateral mu, ipsilateral mu, and ipsilateral beta cycles. These findings show that motor command release coincides with restricted beta rhythm phases, consistent with the notion that sensorimotor rhythm phase shapes the timing of voluntary movement in the healthy human brain.

References

Baker SN, Olivier E, Lemon RN (1997) Coherent oscillations in monkey motor cortex and hand muscle show task-dependent modulation. J Physiol 501:225–241.

Baumgarten TJ, Schnitzler A, Lange J (2015) Beta oscillations define discrete perceptual cycles in the somatosensory domain. Proc Natl Acad Sci U S A 112:12187–12192.

Bell AJ, Sejnowski TJ (1995) An information-maximization approach to blind separation and blind deconvolution. Neural Comput 7:1129–1159.

Berens P (2009) CircStat: a MATLAB toolbox for circular statistics. J Stat Softw 31:1–21.

Berger B, Minarik T, Liuzzi G, Hummel FC, Sauseng P (2014) EEG oscillatory phase-dependent markers of corticospinal excitability in the resting brain. Biomed Res Int 2014:936096.

Bergmann TO, Lieb A, Zrenner C, Ziemann U (2019) Pulsed facilitation of corticospinal excitability by the sensorimotor μ-alpha rhythm. J Neurosci 39:10034–10043.

Busch NA, VanRullen R (2010) Spontaneous EEG oscillations reveal periodic sampling of visual attention. Proc Natl Acad Sci U S A 107:16048–16053.

Busch NA, Dubois J, VanRullen R (2009) The phase of ongoing EEG oscillations predicts visual perception. J Neurosci 29:7869–7876.

Brecht M, Schneider M, Sakmann V, Margrie TW (2004) Whisker movements evoked by stimulation of single pyramidal cells in rat motor cortex. Nature 427:704–710.

Chen RM, Yaseen Z, Cohen LG, Hallett M (1998) Time course of corticospinal excitability in reaction time and self-paced movements. Ann Neurol 44:317–325.

Conway BA, Halliday DM, Farmer SF, Shahani U, Maas P, Weir AI, Rosenberg JR (1995) Synchronization between motor cortex and spinal motoneuronal pool during the performance of a maintained motor task in man. J Physiol 489:917–924.

De Luca CJ, Donald GL, Kuznetsov M, Roy SH (2010) Filtering the surface EMG signal: movement artifact and baseline noise contamination. J Biomech 43:1573–1579.

Di Lazzaro V, Ziemann U (2013) The contribution of transcranial magnetic stimulation in the functional evaluation of microcircuits in human motor cortex. Front Neural Circuits 7:18.

Donoghue T, Haller M, Peterson EH, Varma P, Sebastian P, Gao R, Noto T, Lara AH, Wallis JD, Knight RT, Shestyuk A, Voytek B (2020) Parameterizing neural power spectra into periodic and aperiodic components. Nat Neurosci 23:1655–1665.

Dugué L, Marque P, VanRullen R (2011) The phase of ongoing oscillations mediates the causal relation between brain excitation and visual perception. J Neurosci 31:11889–11893.

Farmer SF, Bremner FD, Halliday DM, Rosenberg JR, Stephens JA (1993) The frequency content of common synaptic inputs to motoneurones studied during voluntary isometric contraction in man. J Physiol 470:127–155.

Ferreri F, Vecchio F, Ponzo D, Pasqualetti P, Rossini PM (2014) Time-varying coupling of EEG oscillations predicts excitability fluctuations in the primary motor cortex as reflected by motor evoked potentials amplitude: an EEG-TMS study. Hum Brain Mapp 35:1969–1980.

Gao R, Peterson EJ, Voytek B (2017) Inferring synaptic excitation/inhibition balance from field potentials. Neuroimage 158:70–78.

Haegens S, Nácher V, Luna R, Romo R, Jensen O (2011) α-Oscillations in the monkey sensorimotor network influence discrimination performance by rhythmical inhibition of neuronal spiking. Proc Natl Acad Sci U S A 108:19377–19382.

Hanes DP, Schall JD (1996) Neural control of voluntary movement initiation. Science 274:427–430.

Hanslmayr S, Volberg G, Wimber M, Dalal SS, Greenlee MW (2013) Prestimulus oscillatory phase at 7 Hz gates cortical information flow and visual perception. Curr Biol 23:2273–2278.

Hussain SJ, Claudino L, Bönstrup M, Norato G, Cruciani G, Thompson R, Zrenner C, Ziemann U, Buch E, Cohen LG (2019) Sensorimotor oscillatory phase–power interaction gates resting human corticospinal output. Cereb Cortex 29:3766–3777.

Hjorth B (1975) An on-line transformation of EEG scalp potentials into orthogonal source derivations. Electroencephalog Clin Neurophysiol 39:526–530.

Hyvarinen A (1999) Fast and robust fixed-point algorithms for independent component analysis. IEEE Trans Neural Netw 10:626–634.

Ibáñez J, Del Vecchio A, Rothwell JC, Baker SN, Farina D (2021) Only the fastest corticospinal fibers contribute to β corticomuscular coherence. J Neurosci 41:4867–4879.

Kerrén C, Linde-Domingo J, Hanslmayr S, Wimber M (2018) An optimal oscillatory phase for pattern reactivation during memory retrieval. Curr Biol 28:3383–3392.

Khademi F, Royter V, Gharabaghi A (2018) Distinct beta-band oscillatory circuits underlie corticospinal gain modulation. Cereb Cortex 28:1502–1515.

Khademi F, Royter V, Gharabaghi A (2019) State-dependent brain stimulation: power or phase? Brain Stimul 12:296–299.

Klimesch W, Russegger H, Doppelmayr M, Pachinger T (1998) A method for the calculation of induced band power: implications for the significance of brain oscillations. Electroencephal Clin Neurophysiol 108:123–130.

Kosciessa JQ, Grandy TH, Garret DD, Werkle-Bergner M (2020) Single-trial characterization of neural rhythms: potential and challenges. Neuroimage 206:116331.

Little S, Brown P (2014) The functional role of beta oscillations in Parkinson's disease. Parkinson's. Rel Disorders 20:S44–S48.

Manning JR, Jacobs J, Fried I, Kahana MJ (2009) Broadband shifts in local field potential power spectra are correlated with single-neuron spiking in humans. J Neurosci 29:13613–13620.

Martin S, Iturrate I, Chavarriaga R, Leeb R, Sobolewski A, Li AM, Zaldivar J, Peciu-Florianu I, Pralong E, Castro-Jiménez M, Benninger D, Vingerhoets F, Knight RT, Bloch J, Millán JDR (2018) Differential contributions of subthalamic beta rhythms and 1/f broadband activity to motor symptoms in Parkinson's disease. NPJ Parkinson's Dis 4:32.

Miller KJ, Hermes D, Honey CJ, Hebb AO, Ramsey NF, Knight RT, Ojemann JG, Fetz EE (2012) Human motor cortical activity is selectively phase-entrained on underlying rhythms. PLoS Comput Biol 8:e1002655.

Mima T, Hallett M (1999) Corticomuscular coherence: a review. J Clin Neurophysiol 16:501–511.

Mitchell MK, Baker MR, Baker SN (2007) Muscle responses to transcranial stimulation depend on background oscillatory activity. J Physiol 583:567–579.

Montemurro MA, Rasch MJ, Murayama Y, Logothetis NK, Panzeri S (2008) Phase-of-firing coding of natural visual stimuli in primary visual cortex. Curr Biol 18:375–380.

Murthy VN, Fetz EE (1992) Coherent 25-to 35-Hz oscillations in the sensorimotor cortex of awake behaving monkeys. Proc Natl Acad Sci U S A 89:5670–5674.

Murthy VN, Fetz EE (1996a) Oscillatory activity in sensorimotor cortex of awake monkeys: synchronization of local field potentials and relation to behavior. J Neurophysiol 76:3949–3967.

Murthy VN, Fetz EE (1996b) Synchronization of neurons during local field potential oscillations in sensorimotor cortex of awake monkeys. J Neurophysiol 76:3968–3982.

Oostenveld R, Fries P, Maris E, Schoffelen JM (2011) FieldTrip: open-source software for advanced analysis of MEG, EEG, and invasive electrophysiological data. Comp Intell Neurosci 2011:156869.

Pellicciari MA, Veniero D, Miniussi C (2017) Characterizing the cortical oscillatory response to TMS pulse. Front Cell Neurosci 11:38.

Pfurtscheller G, Aranibar A (1979) Evaluation of event-related desynchronization (ERD) preceding and following voluntary self-paced movement. Electroencephalog Clin Neurophysiol 46:138–146.

Pfurtscheller G, Lopes da Silva F (1999) Event-related EEG/MEG synchronization and desynchronization: basic principles. Clin Neurophysiol 110:1842–1857.

Pfurtscheller G, Brunner C, Schlögl A, Lopes da Silva F (2006) Mu rhythm (de)synchronization and EEG single-trial classification of different motor imagery tasks. NeuroImage 31:153–159.

Pineda JA (2005) The functional significance of mu rhythms: translating "seeing" and "hearing" into "doing. Brain Res Brain Res Rev 50:57–68.

Pogosyan A, Gaynor LD, Eusebio A, Brown P (2009) Boosting cortical activity at beta-band frequencies slows movement in humans. Curr Biol 19:1637–1641.

Premoli I, Bergmann TO, Fecchio M, Rosanova M, Biondi A, Belardinelli P, Ziemann U (2017) The impact of GABA-ergic drugs on TMS-induced brain oscillations in human cortex. Neuroimage 163:1–12.

Ruzzoli M, Torralba M, Fernández LM, Soto-Faraco S (2019) The relevance of alpha phase in human perception. Cortex 120:249–268.

Romei V, Bauer M, Brooks JL, Economides M, Penny W, Thut G, Driver S, Bestmann S (2016) Causal evidence that intrinsic beta-frequency is relevant for enhanced signal propagation in the motor system as shown through rhythmic TMS. Neuroimage 126:120–130.

Salmelin R, Hari R (1994) Spatiotemporal characteristics of sensorimotor neuromagnetic rhythms related to thumb movement. Neuroscience 60:537–550.

Salmelin R, Hämäläinen M, Kajola M, Hari R (1995) Functional segregation of movement-related rhythmic activity in the human brain. Neuroimage 2:237–243.

Siegel M, Warden MR, Miller EK (2009) Phase-dependent neuronal coding of objects in short-term memory. Proc Natl Acad Sci U S A 106:21341–21346.

Stolk A, Brinkman L, Vansteensel MJ, Aarnoutse E, Leijten FSS, Dijkerman C, Knight RT, de Lange FP, Toni I (2019) Electrocortigraphic dissociation of alpha and beta rhythmic activity in the human sensorimotor system. Elife 8:e48065.

Takahashi N, Moberg S, Zolnik TA, Catanese J, Sachdev RNS, Larkum ME, Jaeger D (2021) Thalamic input to motor cortex facilitates goal-directed action initiation. Curr Biol 31:4148–4155.

Ten Oever S, De Weerd P, Sack AT (2020) Phase-dependent amplification of working memory content and performance. Nat Comm 11:1832.

Ter Wal M, Linde-Domingo J, Lifanov J, Roux F, Kolibius L, Gollwitzer S, Lang J, Hamer H, Rollings D, Sawlani V, Chelvarajah R, Staresina B, Hanslmayr S, Wimber M (2021) Theta rhythmicity governs the timing of behavioral and hippocampal in humans specifically during memory-dependent tasks. Nat Commun 12:7048.

Torrecillos F, Falato E, Pogosyan A, West T, Di Lazzaro V, Brown P (2020) Motor cortex inputs at the optimum phase of beta cortical oscillations undergo more rapid and less variable corticospinal propagation. J Neurosci 40:369–381.

van Elswijk G, Maij F, Schoffelen JM, Overeem S, Stegeman DF, Fries P (2010) Corticospinal beta-band synchronization entails rhythmic gain modulation. J Neurosci 30:4481–4488.

VanRullen R (2016) Perceptual cycles. Trends Cogn Sci 20:723–735.

VanRullen R (2018) Attention cycles. Neuron 99:632–634.

Wischnewski M, Haigh ZJ, Shirinpour S, Alekseichuk I, Opitz A (2022) The phase of sensorimotor mu and beta oscillations has the opposite effect on corticospinal excitability. BioRxiv. doi: 10.1101/2022.02.22.481530.

Womelsdorf T, Schoffelen JM, Oostenveld R, Singer W, Desimone R, Engel AK, Fries P (2007) Modulation of neuronal interactions through neuronal synchronization. Science 316:1609–1612.

Zanos S, Rembado I, Chen D, Fetz EE (2018) Phase-locked stimulation during cortical beta oscillations produces bidirectional synaptic plasticity in awake monkeys. Curr Biol 28:2512–2526.

Zhou B, Lapedriza A, Khosla A, Oliva A, Torralba A (2018) Places: a 10 million image database for scene recognition. IEEE Trans Pattern Anal Mach Intell 40:1452–1464.

Zrenner C, Desideri D, Belardinelli P, Ziemann U (2018) Real-time EEG-defined excitability states determine efficacy of TMS-induced plasticity in human motor cortex. Brain Stimul 11:374–389.